Variability in single-cell oxygen consumption kinetics

Ermes Botte[a,b,1], Yuan Cui[c,d,1], Chiara Magliaro[a,b], Maria Tenje[d], Klaus Koren[e], Andrea Rinaldo[f,g], Roman Stocker[h], Lars Behrendt[c,2,*] and Arti Ahluwalia[a,b,2,*]

[a] Research Centre "E. Piaggio", University of Pisa, Italy

[b] Department of Information Engineering, University of Pisa, Italy

[c] Department of Organismal Biology, Science for Life Laboratory, Uppsala University, Sweden

[d] Department of Material Science and Engineering, Science for Life Laboratory, Uppsala University, Sweden

[e] Aarhus University Centre for Water Technology, Department of Biology, Aarhus University, 8000 Aarhus, Denmark

[f] Laboratory of Ecohydrology ECHO/IIE/ENAC, École Polytechnique Fédérale de Lausanne, Switzerland

[g] Department of Civil, Environmental and Architectural Engineering, University of Padova, Italy

[h] Institute for Environmental Engineering, Department of Civil, Environmental and Geomatic Engineering, ETH Zurich, Zurich, Switzerland

[1] shared first authorship
[2] shared senior authorship

[*] corresponding authors:

Arti Ahluwalia, Research Centre "E. Piaggio" – University of Pisa, Largo Lucio Lazzarino 1, 56125 Pisa, Italy, +39 0502217062; **e-mail**: arti.ahluwalia@unipi.it

Lars Behrendt, Department of Organismal Biology, Environmental Toxicology, Norbyvagen 18A, 75236, Uppsala, Sweden, +46 184712591; **e-mail**: lars.behrendt@scilifelab.uu.se

Keywords: single cells, oxygen metabolism, size-related variability, Michaelis-Menten kinetics, multiparameter identification

Abstract

We combined microfabricated devices with multiparameter identification algorithms to probe the variability in size-dependent oxygen consumption parameters of single human hepatic cells. We demonstrate that single cells exhibit an oxygen-dependent metabolic rate, typical of Michaelis-Menten kinetics, and that their maximal oxygen consumption is significantly lower than that of monolayers or 3D hepatic cell aggregates. Notably, we found that clusters of two or more cells competing for a limited oxygen supply reduced their maximal single-cell consumption rate, highlighting their ability to adapt to local resource availability and the presence of nearby cells. Next, we used our high-throughput approach to characterize the covariance of size and oxygen consumption within a cell population.

The results show that cooperative behaviour emerges in cell clusters, and that single-cell size and metabolism can be described by a lognormal joint probability density. Our study thus serves as a foundation to connect the metabolic activity of single human hepatocytes to their tissue- or organ-level metabolism as well as describe its size-related variability through scaling laws.

Introduction

Biological variability (*i.e.*, the fluctuation of physiological traits among individuals of the same population, also referred to as biological noise) is ubiquitous and can impact phenomena such as metabolic scaling and resilience to environmental perturbations [1, 2]. Variability is often not confined to one parameter but characterized by an interplay between multiple variables within an organism or ecosystem. For instance, it has been suggested that the covariance between individual size and metabolism conditions the ability of living organisms to react to external stimuli (*e.g.*, toxins or drugs) or explain patterns in homeostatic control [1, 3, 4]. Joint variations between physiological parameters can also impact the susceptibility of organisms to diseases and their overall health [5]. Biological variability has been extensively investigated at the molecular level (transcription and expression), but less so at cellular and organismal levels. Investigating individual cells, instead of in tissues or organs, offers the opportunity to characterize variability between individuals to infer dynamics occurring at higher scales of complexity. Single cells also provide a suitable testbed to determine intrinsic size-related variability and its role in metabolic scaling, which has been highlighted as a criterion for translatability of biological parameters from micro-scale i*n vitro* systems to the *in vivo* context [1, 6, 7].

As oxygen (O_2) is at the heart of aerobic metabolism [8, 9], several studies have measured O_2 consumption in individual mammalian cells [10–13]. However, the accuracy, reproducibility, and throughput of O_2 measurements at this scale remain challenging. Mammalian cells possess the ability to modulate their O_2 consumption according to its availability, a process that is, in turn, influenced by numerous factors (*e.g.*, height of culture medium and cell density) [14, 15]. However, many studies assume that cells possess a constant (zero-order) consumption rate which depends only on cell phenotype. The O_2 consumption rate (R_{cell}, in mol s^{-1}) of a single cell as a function of the surrounding O_2 concentration (c, in mol m^{-3}) is typically represented by the Michaelis-Menten (MM) model [16–18] via two parameters: the maximal consumption rate ($sOCR$, in mol s^{-1}) and the MM constant (k_M, in mol m^{-3}).

$$R_{cell} = -sOCR \frac{c}{k_M + c} \qquad (1)$$

k_M corresponds to the concentration at which the consumption rate is half of its maximal value. At high O_2 levels ($c \gg k_M$), the cellular consumption rate saturates at its maximum value (*i.e.*, $R_{cell} \cong -sOCR$). On the other hand, if $c \ll k_M$, the cellular uptake rate depends on the O_2 concentration as $R_{cell} = -\frac{sOCR}{k_M}c$. Hence, a cell with a low k_M value consumes O_2 maximally even at low concentrations, whereas a cell with a high k_M has a low O_2 uptake efficiency (*i.e.*, O_2 levels must be high to achieve near-maximal consumption rates).

Despite the widespread application of Eq. (1) and its relevance to the prediction and understanding of the ability of cells to adapt to environmental conditions, MM parameters for individual mammalian cells have not been measured. Here we present a systematic approach to conduct single-cell measurements of O_2 consumption as described by the MM model. Our primary objective was to estimate the MM kinetic parameters (*i.e.*, $sOCR$ and k_M) and explore their size-related variability in a human hepatic cell line, HepG2 [19]. Using custom glass microwell devices coated with luminescent O_2-sensitive optode materials [20, 21], we isolated single cells or clusters of a few cells (from two to seven) under precisely controlled experimental conditions. Automated fluorescence microscopy was used to perform time-series imaging of the wells to extract cell sizes and O_2 concentration profiles of individual wells. A multiparameter identification procedure [22] was applied to determine MM parameters from these profiles. Through this approach, we were able to estimate single-cell size and metabolic parameters of O_2 as a joint probability distribution and so describe their correlated variability.

This quantitative description of single-cell O_2 consumption allows probing the biophysical basis of cooperative metabolic dynamics, which are only detectable at higher levels of organization. Our

2

study thus offers guidance in the design of *in vitro* or *in silico* cell-based models (*e.g.*, microtissues, organoids) to improve their predictive value in biomedical applications.

Results

Using glass microwell devices (Figure 1A) in conjunction with O_2 sensitive optode chemistry (Figure 1B) we measured a total of 1080 microwells across five independent experiments. Of these, 227 microwells (~ 21%) contained at least one hepatic cell whose O_2 consumption dynamics (Figure 1D) could be recorded without interference from neighbouring wells (see SI, section SI4). The distribution of the number of cells per well (N_{cell}) is reported in Figure 1E. Notably, in more than half of the cases in which cells were present in a microwell (*i.e.*, 119 measurements, ~ 11% of all investigated microwells), a single cell was probed (Figure 1C), while a maximum of seven cells per well was recognized only once.
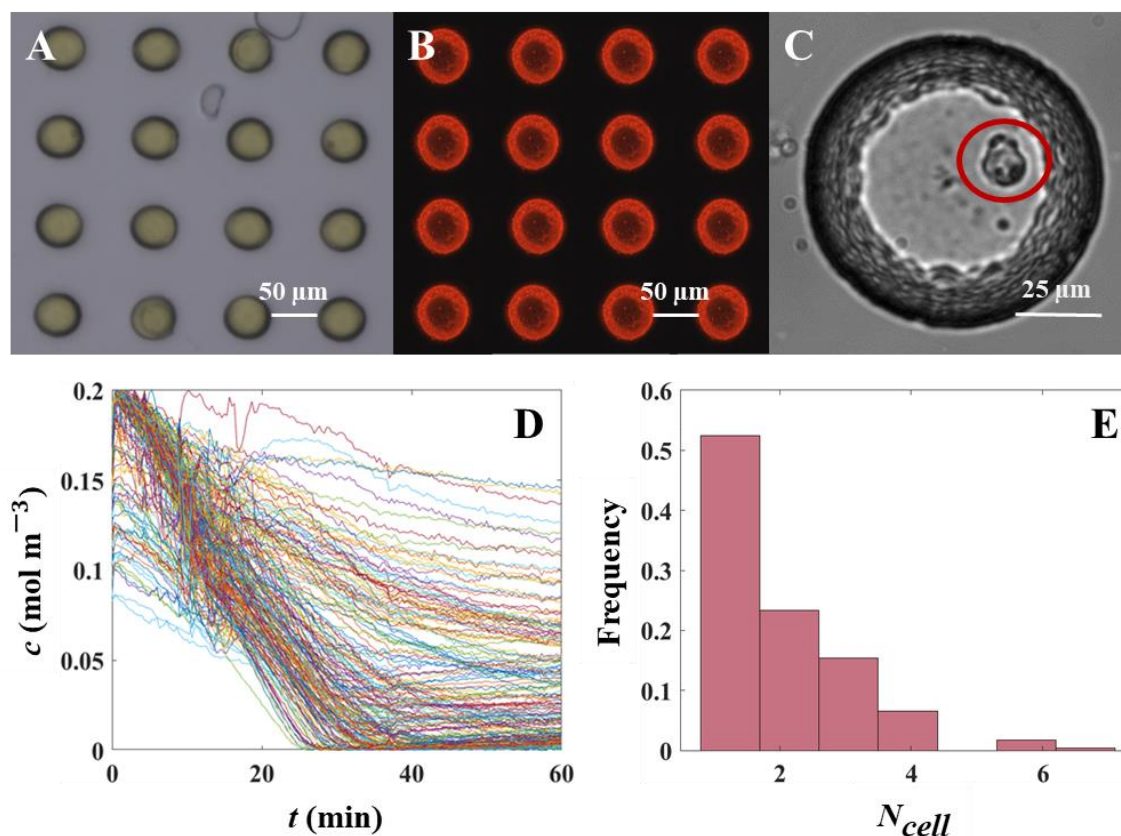

Figure 1. O_2 dynamics of single hepatic cells in glass microwells. (**A***)* Brightifield image of individual microwells with deposited optode chemistry (yellow) in the custom-built glass microwell array. (**B**) Corresponding luminescent response (red) upon exposure to excitation light. (**C**) Image of a single hepatic cell in a microwell with 100 µm diameter. (**D**) O_2 concentration profiles measured in 216 microwells. (**E**) Occupation (N_{cell}) frequency of cells in microwells.

Oxygen consumption kinetics and number of cells per well

The O_2 profiles determined from individual or multiple cells within a glass microwell were used to compute *sOCR* and k_M for cells within each microwell through a multiparameter identification algorithm [22]. The two MM parameters are reported both as overall probability distributions (Figure 2A, 2C) and as a function of N_{cell} (Figures 2B, 2D). While our *sOCR* values are similar to previous estimates for hepatocytes cultured in a hollow fibre bioartificial liver [23], they were significantly

lower (median $sOCR$ = 9.8×10^{-18} mol cell^{-1} s^{-1}) than most of those reported in the literature for hepatocyte monolayers or 3D aggregates (median $sOCR$ = 5.5×10^{-17} mol cell^{-1} s^{-1}, Wilcoxon test, $p < 0.0001$, Figure 3A) [6, 15, 18, 22, 24–26]. Moreover, a Kruskal-Wallis test highlighted significant differences among $sOCR$ values determined for microwells containing a different number of cells ($p < 0.0001$). Specifically, we found that $sOCR$ decreases with increasing N_{cell} (Figure 2B, Spearman coefficient r = -1). This suggests that cells adjust their $sOCR$ when O$_2$ availability is limited because of consumption by other nearby cells.

Our measurements of k_M show a wide distribution, covering three orders of magnitude (Figure 2C), with a significantly higher median (5.3×10^{-2} mol m^{-3}) compared to values previously reported for 2D and 3D hepatic constructs (8.5×10^{-3} mol m^{-3} – Wilcoxon test, $p < 0.0001$) [15, 22]. Approximately 36% of the measured k_M values are comparable to or even higher than the O$_2$ saturation level in water (c_0 = 0.21 mol m^{-3}), suggesting that, once isolated, about a third of the cells do not approach their maximal consumption rate but instead follow first order kinetics. Due to the large variability of k_M, neither a significant correlation with N_{cell} (Spearman coefficient r = -0.086) nor statistical differences among its medians for different N_{cell} values (Kruskal-Wallis test, p = 0.7603) were detected (Figure 2D).
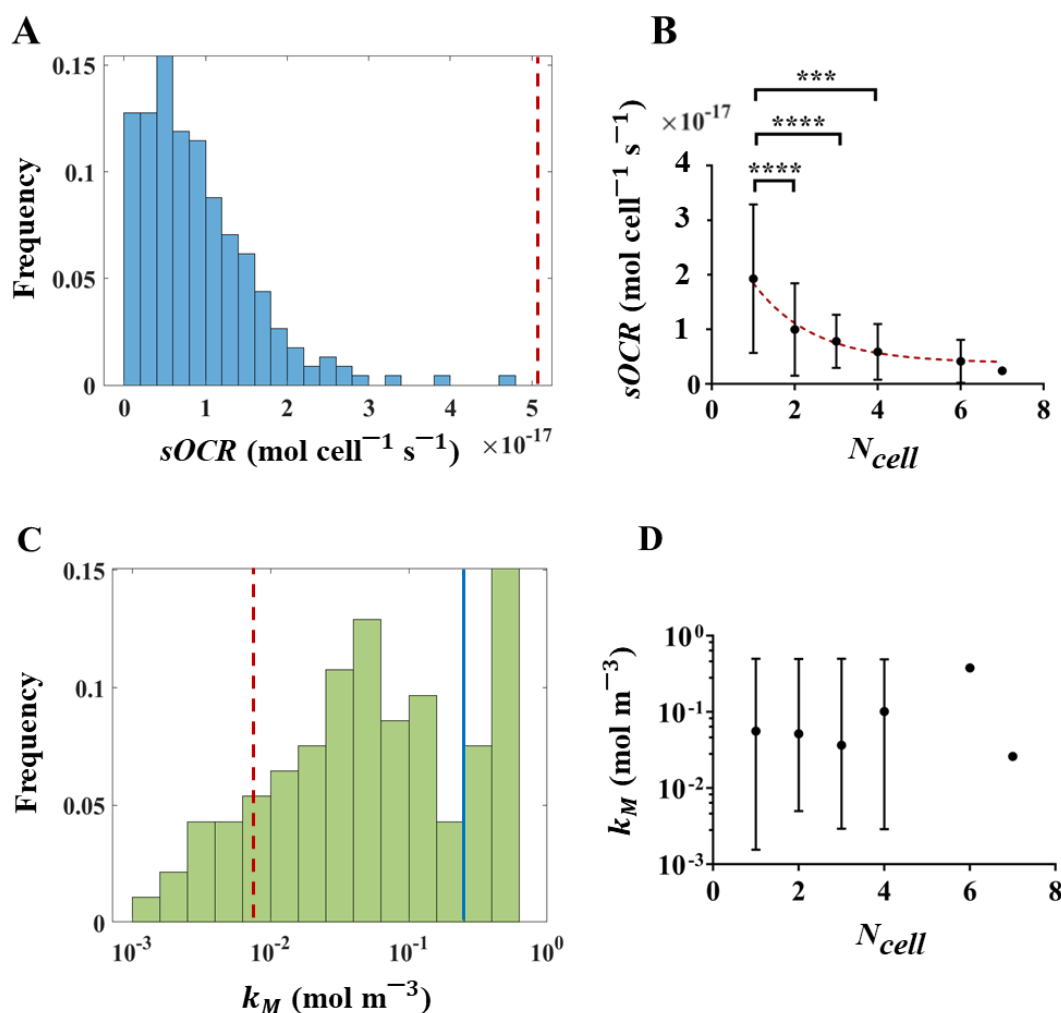

Figure 2. MM kinetic parameters in isolated hepatic cells determined through the multiparameter identification procedure. (A) Relative frequency of $sOCR$ in occupied

microwells. (**B**) Correlation between the number of cells per microwell and the corresponding $sOCR$ value (r = -1), over all occupied microwells. The red dashed curve is a weighted fit of results (one phase exponential decay, R^2 = 0.9797). Pairwise statistical differences computed using Dunn's *post hoc* multiple comparisons are also reported ([***] p < 0.0005, [****] p < 0.0001). (**C**) Relative frequency of k_M in occupied microwells (expressed in logarithmic scale). (**D**) No correlation was observed between k_M and the number of cells per well (r = -0.086). The vertical red dashed lines in (**A**) and (**C**) denote median literature values of $sOCR$ and k_M [13, 16, 20–23], respectively (see Table 1 for a complete list of reported values), while the solid blue line in (**C**) indicates the O_2 saturation level in water (c_0). In (**B**) and (**D**), data are reported as median ± range.

To help distinguish mutual dependencies of $sOCR$ and k_M, MM parameters for all microwells investigated are presented in a scatter plot (Figure 3A). Data points referring to microwells populated by the same number of cells are clustered along the $sOCR$ axis. However, no noticeable separation among groups of points corresponding to different values of N_{cell} with respect to k_M was observed. A correlation analysis indeed suggests that the two MM parameters do not depend on each other (Spearman coefficient r = 0.1608), a finding that is in contrast to previous observations for 2D and 3D aggregates of hepatic cells [22]. For comparison, bulk values for the two kinetic parameters, averaged over several cells as reported in the literature [6, 15, 18, 22–26], are also indicated in Figure 3A and listed in Table 1.

Joint measurements of single-cell size and metabolism
Immediately after each experiment, HepG2 cells were stained with Trypan Blue, which allowed determining single-cell sizes from projected cell areas. From this data, we estimated the joint distribution of single-cell size and $sOCR$ (Figure 3B). The Henze-Zirkler test (α = 0.01) demonstrated that the sample can be described by a lognormal joint probability density function (p = 0.0344). Further confirmation of lognormality was provided by independent optical measurements of dry mass of individual HepG2 cells – performed by means of quantitative phase imaging – which coherently displayed a marginal distribution with a lognormal shape (see SI, section SI6).
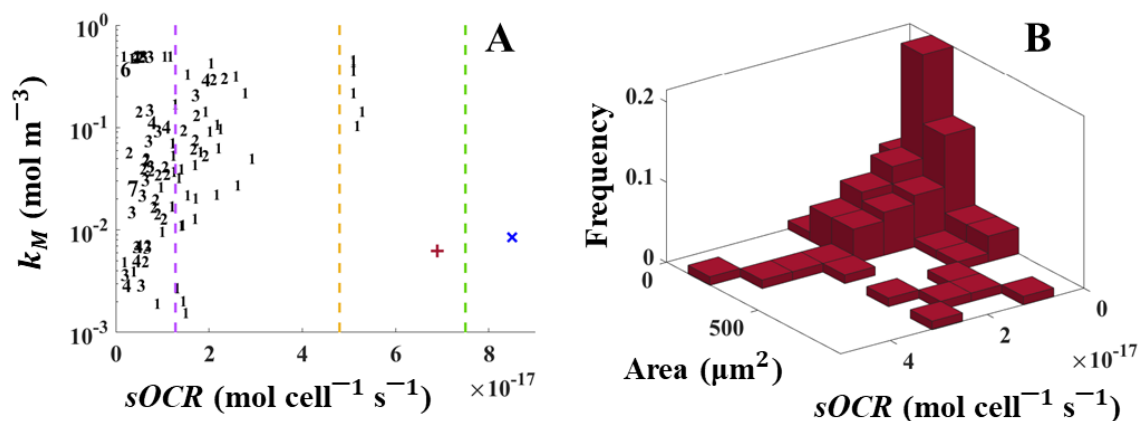

Figure 3. Mutual dependency of MM parameters and the size-related variability of O_2 consumption in single human hepatic cells. (A) Scatter plot of measured $sOCR$ and k_M values. The Spearman coefficient indicates that the two parameters do not exhibit any correlation (r = 0.1608). Each data point is denoted by a number, which corresponds to the value of N_{cell} for that data point. The red plus [15] and the blue cross [22] are median bulk values from the literature (see Table 1). Dashed lines indicate $sOCR$ values from previous studies assuming zero-order kinetics for O_2 consumption (yellow: [25], green: [26], purple: [23]). Note that k_M values are reported in logarithmic scale. (**B**) Joint distribution of single-cell size (*i.e.*, projected area) and O_2 metabolism (*i.e.*, $sOCR$), expressed as relative frequency of occurrence.

Table 1. Values of $sOCR$ and k_M from previous studies as bulk averages of human hepatic cell aggregates. Median values are reported for studies investigating different cell densities [15, 22]. For references which consider zero-order consumption kinetics [23–26], k_M values are not reported (NA).

Aggregate type	$sOCR$ (×10^{-18} mol cell^{-1} s^{-1})	k_M (×10^{-3} mol m^{-3})	Reference
Isolated single cell	9.8	53	This study
Cell-laden hydrogel (3D)	69	6.2	[15]
Cell monolayer (2D)	37	5.0	[22]
Cell-laden spheroid (3D)	85	8.5	[22]
Bioartificial liver (3D)	13	NA	[23]
Cell monolayer (2D)	55	NA	[24]
Cell-laden hydrogel (3D)	48	NA	[25]
Microcarrier (3D)	78	NA	[26]

Discussion

Here we report on the characterization of O_2 metabolism in single human hepatic cells. Using microfabricated glass devices, coated with O_2-sensitive optodes, one or a few cells were seeded in each microwell, enabling the precise measurement of O_2 consumption over time as a function of the number of cells per microwell. These data were then exploited in a multiparameter identification algorithm [22] to characterize the cellular O_2 consumption kinetics according to the MM model (Eq. (1)).

Using this integrated *in silico-in vitro* approach, we demonstrate that isolated HepG2 cells have a lower $sOCR$ compared to values previously reported for 2D or 3D aggregates of the same cell type in comparable environmental conditions (Figure 2A) [15, 22, 24–26]. Additionally, our data show higher k_M values compared to those reported in earlier studies (Figure 2C) [15, 22]. This suggests that cells modulate their O_2 metabolism when isolated as individuals or in clusters of a few cells. In addition, the decrease in $sOCR$ with increasing number of cells per microwell, N_{cell}, shows that the modulation occurs as a function of both the local O_2 concentration and the presence of other cells (Figure 2B). This behaviour mirrors observations on hepatocytes in 2D and 3D aggregates [22] and could be interpreted as an effect of cooperation among individual cells that coexist in a microenvironment where a limited resource is shared. However, contrary to what we previously observed for hepatic cells in 2D and 3D [22], the adaptive behaviour in isolated cells appears not to affect the O_2 uptake efficiency, since k_M is not dependent on N_{cell} (Figure 2D), and the two parameters are not significantly correlated (Figure 3A). It is worth noting that the identification of k_M is influenced by the ability of the microwell system to effectively achieve hypoxic steady-state conditions. Thus, although the optodes are highly sensitive at low O_2 concentrations (see SI, section SI3), even slight variations of stationary O_2 levels can influence the estimation of k_M and widen its distribution. Indeed, precisely characterizing k_M is a well-known challenge because of the sensitivity of estimated values to experimental conditions [22, 27, 28], which might ultimately mask potential trends. Nonetheless, the estimations of $sOCR$ are statistically robust and not impacted by the uncertainty in k_M, as shown in Figure 2B.

The throughput of our approach allowed us to measure the correlated variability of cell size and maximal O_2 consumption rate (*i.e.*, $sOCR$) and describe their joint frequency distribution (Figure

3B). This outcome successfully overcomes the challenge of jointly investigating individual size and metabolism, a hurdle previously encountered by our group and others [3]. Although further experiments are required to fully capture the covariance between single-cell size and O_2 consumption [1], our study is the first size-metabolic rate distribution based on joint experimental datasets reported so far. Notably, our analysis demonstrates that the sample is extracted from a population characterized by a lognormal multivariate function. Lognormally-distributed marginal probabilities have been commonly observed for organismal sizes [29], but they have not been explicitly reported for metabolic rates.

Characterizing the covariance of single-cell size and metabolic parameters – as achieved here – is crucial to comprehensively describe the metabolic dynamics (*e.g.*, O_2 consumption) of human hepatocytes in isolation. It also paves the way to link these dynamics to the tissue or organ levels and to interpret behaviours emerging at higher scales such as cooperation or size-related scaling. A direct application of this work is the development of engineered cellular systems capable of recapitulating the heterogeneity of single-cell metabolic phenotypes. This may enhance precision medicine approaches, drug development strategies or (eco)toxicological assessments. Besides the biomedical field, the proposed methodology is also of general interest as it provides a powerful framework for systematically characterizing O_2 metabolism and its size-related fluctuations in other single-cell scenarios, ranging from the photosynthetic activity of marine microorganisms to the evaluation of the impact of chemicals or environmental stressors on single-cell respiration.

Materials and Methods

Microwell devices for single-cell isolation and oxygen sensing
Single cells or small clusters of cells were isolated in a custom-built microwell array (see the schematic in Figure 4 and SI, Figure S2). The array consists of a standard borosilicate glass slide with geometrically arranged microwells (100 columns ✕ 250 rows, $n = 25000$ microwells) fabricated via standard dry etching techniques. The microfabrication procedure for this device is summarised in the Supporting Information (SI, Figure S1), and Table S1 reports relevant technical features of the dry etching process and geometric specifications of the array customized to match the size of human hepatic cells and to minimize optical and diffusional crosstalk between microwells.
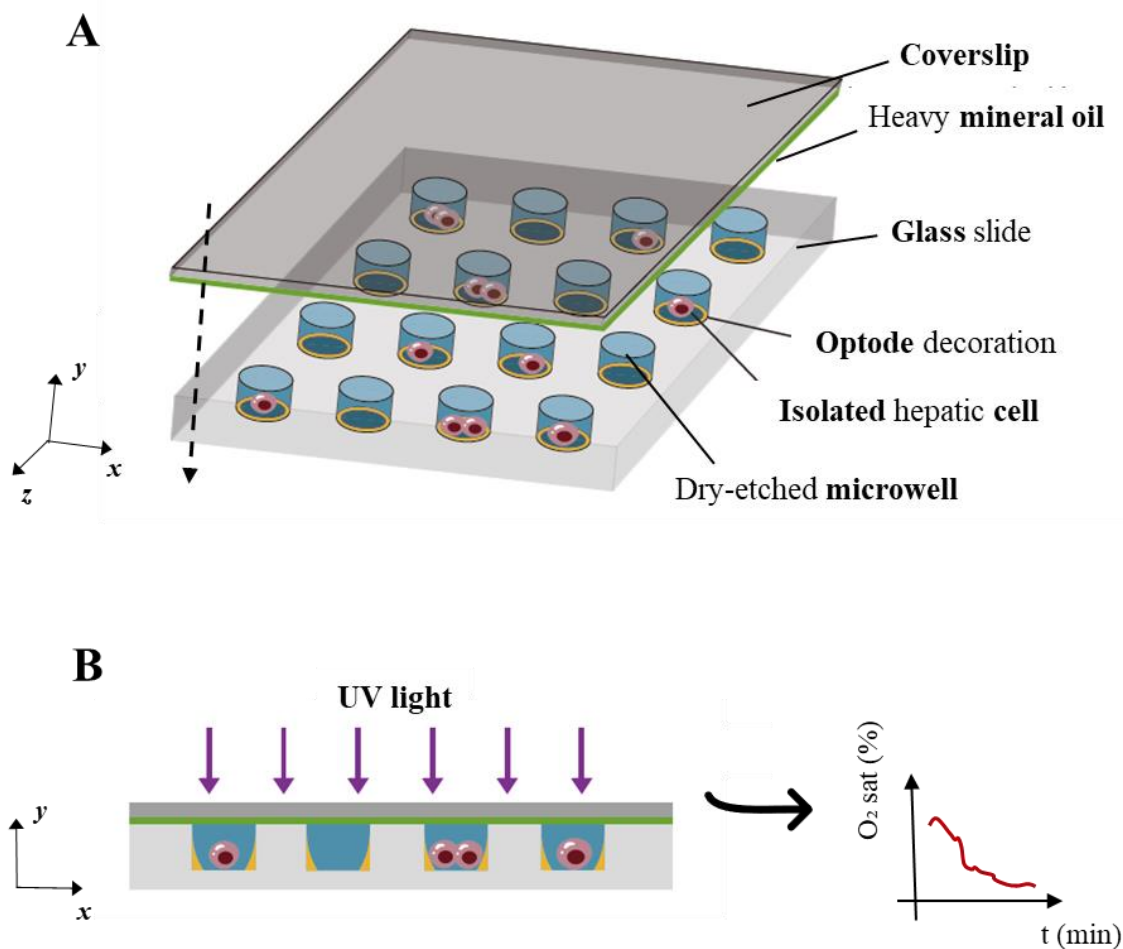
Figure 4. **Schematic of the assembled glass microfluidic device**. **(A)** Microwells coated with optode chemistry are seeded with hepatic cells suspended in culture medium, and subsequently the device is overlaid with a glass coverslip coated in heavy mineral oil. This oil interface reduces lateral (*i.e.*, inter-well) O_2 diffusion so that the microwells effectively reach hypoxic conditions. **(B)** Once sealed, the system is exposed to short pulses of UV light and the resulting luminescence emission from optodes is detected over time to derive O_2 concentrations across microwells. Inset: a typical O_2 concentration profile obtainable by monitoring optode response in an individual microwell where at least one cell is settled.

Optode sensor composition, deposition and calibration
Composition. Quenching-based luminescent optode materials were chosen for O_2 sensing as they are characterized by a high spatial resolution and short response time, as required for single-cell O_2 consumption rate measurements [30, 31]. The deposited optode material was composed of platinum(II)-5,10,15,20-tetrakis-(2,3,4,5,6–pentafluorophenyl)-porphyrin (PtTFPP), polystyrene (PS) and MACROLEX® yellow 10GN (MY) dissolved in toluene. Here, PtTFPP is the O_2-sensitive dye whereas MY acts as a reference (*i.e.*, O_2-insensitive) dye. Both dyes are excited using UV light (λ = 396 nm) and emit red luminescence (PtTFPP, $\lambda \geq 650$ nm) or green luminescence (MY, λ = 507 nm) in an O_2 concentration-dependent manner [31] or at a constant intensity, respectively. The ratio of red-to-green (R/G) emission intensities thus represents a robust O_2-dependent signal, with minimal noise from environmental artefacts (*e.g.*, sensor bleaching) and, with appropriate calibration, allows for relating to O_2 contents within individual microwells.

8

Deposition. To deposit the optode material, a 10% w/v solution of PS in toluene containing 0.15 g/L of both MY and PtTFPP was spread on the glass microwell array via a pipette. The homogeneity of the optode coating was assessed by profilometry (see SI1 for details), which revealed that it had a nominal thickness of 5 µm and was most uniform in the central region of the array. Therefore, we prioritized this central area (containing at least 200 microwells) for seeding cells and investigating their O_2 consumption. As the deposited optode material is hydrophobic, the array was briefly treated with O_2 plasma (Zepto, Diener electronic, Ebhausen, Germany) for 10 s at 0.4 mbar and 50% intensity to promote filling of microwells with culture medium and assist in cell adhesion. This plasma treatment did not affect the response of optode materials to O_2 (see SI2 for details). To avoid undesired background fluorescence, the optode material deposited outside of the microwells was removed using a scalpel. This process resulted in two regions with different wettability, *i.e.*, (i) hydrophilic microwells containing a layer of optode material (yellow regions in the inset of Figure 1A) surrounded by (ii) hydrophobic glass (gray regions in the inset of Figure 1A).

Calibration. Following optode deposition, a calibration curve was constructed by averaging data acquired from 216 central microwells (see SI1 for details). To perform calibration measurements, the optode-coated array was placed into a gas-impermeable chamber with a transparent window for image acquisition. The chamber was placed in a microscopy incubator (Okolab srl, Pozzuoli, Italy) maintained at 37°C, to avoid temperature fluctuations, which might influence optode responses (Figure S2). Optode emissions were recorded via a fully automated fluorescence microscope (Nikon Ti2-*E*, Nikon, Tokyo, Japan) equipped with an RGB camera (DFK 33UX264 colour industrial camera, The Imaging Source) and a LED excitation light (Spectra X, Lumencor, OR, USA).

Calibration was performed by introducing gases at known levels of O_2 saturation. Specifically, the R/G in totally anoxic conditions (R/G_0) was measured by exposing the device first to pure nitrogen (N_2) and thereafter to compressed air (*i.e.*, 21% O_2) to obtain 100% air saturation (R/G_{100}), corresponding to an equilibrium concentration in aqueous media equal to c_0. Images of single microwells were acquired with a 40× objective. All other imaging parameters were set as listed in Table 1 for monitoring cellular O_2 consumption. The measurement was used to derive the Stern-Volmer (SV) quenching constant [31] (k_{SV}, expressed in 1/% air sat.) of the array as follows.

$$k_{SV} = \frac{1}{100}\left(\frac{R/G_0}{R/G_{100}} - 1\right)$$ (2)

Calibration curves were also estimated in liquid phase (*i.e.*, cell culture medium) and compared to those obtained for corresponding microwell arrays using gases (see SI2 for details). No significant differences emerged between liquid phase and gas phase calibrations, and hence we routinely relied on the more convenient gas calibration prior to each experiment. Further, we ensured that optode bleaching was negligible in the timeframe of our single-cell O_2 consumption tests (see SI3 for details). Finally, experiments were conducted to determine the extent of optical crosstalk between microwells and to define inter-well distance and cell occupancy (see SI4 for details).

Single-cell oxygen measurements

Cell preparation. Human hepatic cells from hepatocellular carcinoma (HepG2 cells, ATCC, Manassas, Virginia, USA) were maintained in T25 flasks (Sarstedt, Numbrecht, Germany) under standard conditions (37 °C, 95% humidity, 5% CO_2) and supplied with fresh Dulbecco's Modified Eagle Medium (DMEM, Sigma-Aldrich, St Louis, Missouri, USA) every 3 days. Before experiments, cells were detached with trypsin-EDTA (Lonza, Basel, Switzerland).

After optode calibration, the central area of the microwell array was overlaid with a thick poly-dimethyl-siloxane (PDMS) frame into which 500 µL of cell suspension in DMEM was pipetted (Figure 1B). This allowed control of the seeding density and ensured that cells were confined to the region where the optode coating was determined to be homogeneous. Experiments were performed with different seeding densities, ranging from 2×10^3 cells mL^{-1} up to 10^6 cells mL^{-1}. The former resulted in an optimal trade-off between an acceptable number of microwells containing

9

single cells and minimal lateral O_2 diffusion between neighbouring microwells. Following cell seeding, the device was incubated overnight to allow cell adhesion to the microwells (inset in Figure 1B).

Monitoring single-cell consumption. Just before the single-cell O_2 consumption experiments, the culture medium within the PDMS frame was changed and 60 µL of fresh DMEM were dispensed into the microwells. Then, the PDMS frame was removed and microwells seeded with cells were covered with a coverslip, which was affixed to the array via both paperclips and magnets (Figure 1A). A thin coating of heavy mineral oil (Sigma-Aldrich) was applied to the underside of the coverslip to isolate the microwells from environmental O_2 (Figure 4) and to define the initial and boundary conditions of the system. Mineral oil has a significantly lower O_2 diffusion coefficient than aqueous media [32] and effectively seals off the array from ambient O_2, allowing a hypoxic steady state to be reached – a necessary condition to properly characterize the MM consumption kinetics, particularly k_M (see subsection *Modelling single-cell consumption)*. The ratio of mineral oil to cell culture media was optimized to ensure maximal phase separation and minimize lateral (*i.e.*, inter-well) O_2 diffusion and, at the same time, guarantee that cells are exposed to the medium phase within microwells (see SI5 for details). Image acquisition was started immediately after device assembly to ensure rapid monitoring of O_2 dynamics (*i.e.*, from the initial condition of maximum O_2 in the medium to the achievement of stationary hypoxia, defined as $c \leq 0.04$ mol m^{-3} [33]). Measurement duration and sampling frequency were set according to instrument limits and modelling considerations (see subsection *Modelling single-cell consumption*). The O_2 dynamics associated with cell consumption were measured by repeatedly scanning the central area containing cells, using large area scanning mode. The large image acquisition parameters are listed in Table 2.

Following each experiment, 30 µL of trypan blue dye (0.4% w/v solution, Sigma-Aldrich) was gently pipetted through the gap between the microwell array and the coverslip. Trypan blue was left to diffuse over the array for about 10 min, then a brightfield large image was acquired setting the same scanning pathway as used during experiments. This procedure enabled identifying N_{cell} in each microwell and estimating cell size (*i.e.*, the projected area) using ImageJ [34].

Table 2. Experimental parameters for O_2 sensing, using a Nikon Ti2-*E* automated fluorescence microscopy system.

Parameter	Numerical value
Magnification	10×
Large image size (n×m)	6×6
Time scale (t_{end})	1 h
Time resolution (Δt)	20 s
Excitation light wavelength	396 nm
Excitation light intensity	20% of maximum intensity*
Excitation duration	50 ms

*To achieve optimal saturation of the sensing dye, the intensity of the excitation light was coherently adjusted for each round of calibration and subsequent experiment.

Determination of concentration profiles. Time series of large images were processed exploiting algorithms purposely developed in Matlab (R2021b, MathWorks, Massachusetts, USA). Briefly, each RGB image was segmented by means of customized thresholding to distinguish PtTFPP-decorated microwells from the background. This allowed for the computation of the pixel-by-pixel R/G. Finally, for each microwell, R/G profiles were determined over time by averaging over pixels belonging to the same microwell. This allowed for conversion of R/G signals into O_2 concentrations using previously established calibration curves.

Modelling single-cell consumption. Leveraging analytical considerations and bearing in mind that neither cell location nor the number of cells per well (N_{cell}) can be determined *a priori*, we established the duration (t_{end}) and sampling frequency (f) of measurements based on the experimental setup. From a modelling point of view, each microwell is a region of the space governed by the reaction-diffusion equation (Eq. (3)):

$$\frac{\partial c}{\partial t} = D\nabla^2 c + R \tag{3}$$

where $c = c(x,y,z,t)$ [mol m^{-3}] is the O$_2$ concentration field in the microwell, D [m^2 s^{-1}] is the diffusion constant of O$_2$ and $R = R(x,y,z,t)$ [mol m^{-3} s^{-1}] is the O$_2$ production/consumption rate per unit volume. In the case of consumption, R is negative and can be described as a function of the single-cell MM consumption rate (R_{cell}) defined in Eq. (1). Thus:

$$R = \rho_{cell} R_{cell} \tag{4}$$

where ρ_{cell} [cell m^{-3}] is the cell density in the microwell volume. Given that cell and microwell sizes are comparable, and assuming that O$_2$ consumption is uniform in the cell volume – and hence in the well domain – the cell density can be expressed as $\rho_{cell} = {N_{cell}}/{V_{well}}$ (with V_{well} indicating the microwell volume, Table S1). As the silicone oil layer is considered impermeable to O$_2$, there is no flux at the oil/air boundary, likewise at the microwell walls or – given the homogeneity of consumption in the volume – within the domain. These assumptions imply that the O$_2$ concentration field in the microwell depends only on time ($c(x,y,z,t) = c(t)$), and the governing equation can be simplified as $\frac{\partial c}{\partial t} = R$. In these conditions, a suitable duration for monitoring O$_2$ consumption to hypoxia within each microwell was estimated based on the characteristic reaction time, τ_r:

$$\tau_R = \frac{k_M + c_0}{\rho_{cell} * sOCR} \tag{5}$$

where conditions of O$_2$ saturation (*i.e.*, $c = c_0$, see Table 3) and N_{cell} = 1 were assumed. These are cautious choices leading to the longest τ_R possible for the system, guaranteeing that the consumption dynamics are fully captured. Typical literature values were then used for $sOCR$ and k_M [6, 18, 23, 24], giving τ_R = 678.4 s. Thus, experiments were set with $t_{end} \geq 5\tau_R$ and $f \geq 10/\tau_R$.

Kinetic parameter identification
Experimentally measured O$_2$ concentration profiles constituted the input datasets for the multiparameter identification algorithm reported in [22]. Briefly, values of *sOCR* and k_M were estimated comparing the O$_2$ dynamics measured in each microwell containing cells to those predicted *in silico* by modelling the system according to Eqs. (3) and (4). A model governed by the dimensionless form of Eq. (3) was iteratively solved for each specific microwell, taking N_{cell} from the trypan blue-stained image and parameters listed in Table 2 into account.

$$\frac{\partial \gamma}{\partial T} = -\frac{\tau_R * \rho_{cell} * sOCR * \gamma}{c_0 \left({k_M}/{c_0} + \gamma\right)} \tag{6}$$

In Eq. (6), $\gamma = c/c_0$ and $T = t/\tau_R$ are the non-dimensional concentration and time, respectively. Considering Eq. (5), the dimensionless equation implemented for simulating O_2 consumption in the well is the following:

$$\frac{\partial \gamma}{\partial T} = -N_{cell} \frac{\left(k_M/c_0 + 1\right)\gamma}{\left(k_M/c_0 + \gamma\right)} \qquad (7)$$

The multiparameter identification algorithm described in [22] was used to estimate the MM parameters through Eq. (7). Although the equation does not explicitly depend on $sOCR$, the latter determines the time scale of the solution, given the definition provided for the dimensionless time T.

Statistical analysis and software
Numerical values of consumption parameters identified for microwells as a function of N_{cell} were compared by means of a non-parametric Kruskal-Wallis test and pairwise *post hoc* Dunn's multiple comparisons. Non-linear correlation (*i.e.*, non-parametric Spearman coefficient) of $sOCR$ and k_M with respect to N_{cell} as well as with each other was also tested. Overall statistical differences between the MM parameters estimated here and typical literature values were assessed for both $sOCR$ and k_M using a non-parametric Wilcoxon signed-rank test. Furthermore, the joint distribution of single-cell size and $sOCR$ was tested for both normality and lognormality via the Henze-Zirkler multivariate normality test performed on the original and log-transformed dataset, respectively.
Image processing, simulation of O_2 transport and consumption and multiparameter identification were implemented in Matlab (R2021b), while GraphPad Prism (version 7, GraphPad Software, California USA) was used to perform all statistical analyses.

Table 3. Initial condition and range of parametric sweep implemented for simulating O_2 dynamics within a microwell where N_{cell} cells have settled.

Parameter	Numerical value	Description
c_0	0.2 mol m^{-3} ([18])	Initial condition of O_2 saturated-culture medium
$sOCR$	[10^{-18}; 10^{-16}] mol cell^{-1} s^{-1} (deduced from [18, 35])	Initial range of parametric sweep
k_M	[10^{-3}; 10^{-1}] mol m^{-3} (deduced from [17, 18, 35])	Initial range of parametric sweep

Author Contributions: AA and LB conceived the study and supervised the research and manuscript editing. EB and YC conducted experiments and performed image processing and data analysis. All authors contributed to data interpretation. EB drafted the manuscript, and all authors reviewed it as well as agreed to its submission.

Competing Interest Statement: The authors have no competing interests to declare.

References
1. Botte E, Biagini F, Magliaro C, et al (2021) Scaling of joint mass and metabolism fluctuations in in silico cell-laden spheroids. Proc Natl Acad Sci 118:e2025211118. https://doi.org/10.1073/PNAS.2025211118
2. Frankham R (2005) Genetics and extinction. Biol Conserv 126:131–140. https://doi.org/10.1016/j.biocon.2005.05.002
3. Zaoli S, Giometto A, Marañón E, et al (2019) Generalized size scaling of metabolic rates based on single-cell measurements with freshwater phytoplankton. Proc Natl Acad Sci U S A 116:17323–17329. https://doi.org/10.1073/pnas.1906762116
4. Jung SK, Kauri LM, Qian WJ, Kennedy RT (2000) Correlated oscillations in glucose consumption, oxygen consumption, and intracellular free Ca2+ in single islets of Langerhans. J Biol Chem 275:6642–6650. https://doi.org/10.1074/jbc.275.9.6642
5. Lu YF, Goldstein DB, Angrist M, Cavalleri G (2014) Personalized medicine and human genetic diversity. Cold Spring Harb Perspect Med 4:1–12. https://doi.org/10.1101/cshperspect.a008581
6. Ahluwalia A (2017) Allometric scaling in-vitro. Sci Rep 7:1–7. https://doi.org/10.1038/srep42113
7. Magliaro C, Rinaldo A, Ahluwalia A (2019) Allometric Scaling of physiologically-relevant organoids. Sci Rep 9:1–8. https://doi.org/10.1038/s41598-019-48347-2
8. Rose S (1999) The chemistry of life
9. Roussakis E, Li Z, Nichols AJ, Evans CL (2015) Oxygen-Sensing Methods in Biomedicine from the Macroscale to the Microscale. Angew Chemie Int Ed 54:8340–8362. https://doi.org/10.1002/ANIE.201410646
10. Molter TW, McQuaide SC, Suchorolski MT, et al (2009) A microwell array device capable of measuring single-cell oxygen consumption rates. Sens Actuators B Chem 135:678. https://doi.org/10.1016/J.SNB.2008.10.036
11. Hu A, Qiu R, Wu Z, et al (2010) Using micro-patterned sensors and cell self-assembly for measuring the oxygen consumption rate of single cells. J Micromechanics Microengineering 20:095017. https://doi.org/10.1088/0960-1317/20/9/095017
12. Kelbauskas L, Glenn H, Anderson C, et al (2017) A platform for high-throughput bioenergy production phenotype characterization in single cells. Sci Reports 2017 71 7:1–13. https://doi.org/10.1038/srep45399
13. Hartmann FJ, Mrdjen D, McCaffrey E, et al (2021) Single-cell metabolic profiling of human cytotoxic T cells. Nat Biotechnol 39:186–197. https://doi.org/10.1038/s41587-020-0651-8
14. Peniche Silva CJ, Liebsch G, Meier RJ, et al (2020) A New Non-invasive Technique for Measuring 3D-Oxygen Gradients in Wells During Mammalian Cell Culture. Front Bioeng Biotechnol 8:1–12. https://doi.org/10.3389/fbioe.2020.00595
15. Magliaro C, Mattei G, Iacoangeli F, et al (2019) Oxygen Consumption Characteristics in 3D Constructs Depend on Cell Density. Front Bioeng Biotechnol 7:251. https://doi.org/10.3389/fbioe.2019.00251
16. Michaelis L, Menten M (1913) The kinetics of the inversion effect. Biochem 49:333–369
17. Allen JW, Bhatia SN (2003) Formation of steady-state oxygen gradients in vitro: Application to liver zonation. Biotechnol Bioeng 82:253–262. https://doi.org/10.1002/BIT.10569
18. Mattei G, Giusti S, Ahluwalia A (2014) Design Criteria for Generating Physiologically Relevant In Vitro Models in Bioreactors. Processes 2:548–569. https://doi.org/10.3390/pr2030548
19. Adeva-Andany MM, Pérez-Felpete N, Fernández-Fernández C, et al (2016) Liver glucose

metabolism in humans. Biosci Rep 36:416. https://doi.org/10.1042/BSR20160385/56473

20. Merl T, Koren K (2020) Visualizing NH3 emission and the local O2 and pH microenvironment of soil upon manure application using optical sensors. Environ Int 144:106080. https://doi.org/10.1016/j.envint.2020.106080

21. Scilipoti S, Koren K, Risgaard-Petersen N, et al (2021) Oxygen consumption of individual cable bacteria. Sci Adv 7:1–6. https://doi.org/10.1126/sciadv.abe1870

22. Botte E, Mancini P, Magliaro C, Ahluwalia A (2023) A sense of proximity: cell packing modulates oxygen consumption. APL Bioeng 7:

23. Patzer JF (2004) Oxygen Consumption in a Hollow Fiber Bioartificial Liver - Revisited. Artif Organs 28:83–98. https://doi.org/10.1111/j.1525-1594.2004.07150.x

24. Wagner BA, Venkataraman S, Buettner GR (2011) The rate of oxygen utilization by cells. Free Radic Biol Med 51:700–712. https://doi.org/10.1016/j.freeradbiomed.2011.05.024

25. Nyberg SL, Remmel RP, Mann HJ, et al (1994) Primary hepatocytes outperform Hep G2 cells as the source of biotransformation functions in a bioartificial liver. Ann Surg 220:59

26. Smith MD, Smirthwaite AD, Cairns DE, et al (1996) Techniques for measurement of oxygen consumption rates of hepatocytes during attachment and post-attachment. Int J Artif Organs 19:36–44. https://doi.org/10.1177/039139889601900106

27. Rees KCJ Van (1994) MICHAELIS-MENTEN KINETICS: CALCULATION AND USE IN NUTRIENT UPTAKE MODELS. Newzeal J For Sci 24:226–233

28. Gattu S, Crihfield CL, Holland LA (2017) Microscale Measurements of Michaelis-Menten Constants of Neuraminidase with Nanogel Capillary Electrophoresis for the Determination of the Sialic Acid Linkage. Anal Chem 89:929–936. https://doi.org/10.1021/ACS.ANALCHEM.6B04074/ASSET/IMAGES/LARGE/AC-2016-040745_0007.JPEG

29. Giometto A, Altermatt F, Carrara F, et al (2013) Scaling body size fluctuations. Proc Natl Acad Sci U S A 110:4646–50. https://doi.org/10.1073/pnas.1301552110

30. Ramamoorthy R, Dutta PK, Akbar SA (2003) Oxygen sensors: Materials, methods, designs and applications. J Mater Sci 2003 3821 38:4271–4282. https://doi.org/10.1023/A:1026370729205

31. Quaranta M, Borisov SM, Klimant I (2012) Indicators for optical oxygen sensors. Bioanal Rev 4:115. https://doi.org/10.1007/S12566-012-0032-Y

32. Stokes YM (2009) Quantifying oxygen diffusion in paraffin oil used in oocyte and embryo culture. Mol Reprod Dev 76:1178–1187. https://doi.org/10.1002/MRD.21089

33. Berger E, Magliaro C, Paczia N, et al (2018) Millifluidic culture improves human midbrain organoid vitality and differentiation. Lab Chip 18:3172–3183

34. Schneider CA, Rasband WS, Eliceiri KW (2012) NIH Image to ImageJ: 25 years of image analysis. Nat Methods 2012 97 9:671–675. https://doi.org/10.1038/nmeth.2089

35. Mattei G, Magliaro C, Giusti S, et al (2017) On the adhesion-cohesion balance and oxygen consumption characteristics of liver organoids. PLoS One 12:e0173206. https://doi.org/10.1371/journal.pone.0173206